Received: 13 October 2023 | Accepted: 12 June 2024 | Published online: 23 July 2024

DOI: 10.1002/saj2.20732

Soil Science Society of America Journal

ORIGINAL ARTICLE

Fundamental Soil Science

Assessing decadal soil redistribution rates using $^{239+240}$Pu across diverse lithologies in Southeast Alaska

Raquel Portes[1,2] | **Diogo Spinola**[2,3,8] | **Michael E. Ketterer**[4] | **Markus Egli**[5] | **Rebecca A. Lybrand**[6] | **Jennifer Fedenko**[7] | **Frances Biles**[2] | **Thomas P. Trainor**[8] | **Ashlee Dere**[9] | **David V. D'Amore**[2]

[1]Department of Geography, Earth and Environmental Sciences, University of Northern British Columbia, Prince George, British Columbia, Canada

[2]Forest Service, U.S. Department of Agriculture, Pacific Northwest Research Station, Juneau, Alaska, USA

[3]Department of Ecosystem Science and Management, University of Northern British Columbia, Prince George, Canada

[4]Department of Chemistry and Biochemistry, Northern Arizona University, Flagstaff, Arizona, USA

[5]Department of Geography, University of Zurich, Zurich, Switzerland

[6]Department of Land, Air & Water Resources, University of California, Davis, Davis, California, USA

[7]Department of Crop and Soil Science, Oregon State University, Corvallis, Oregon, USA

[8]Department of Chemistry and Biochemistry, University of Alaska Fairbanks, Fairbanks, Alaska, USA

[9]Department of Geography and Geology, University of Nebraska, Omaha, Nebraska, USA

Correspondence

Raquel Portes, Department of Geography, Earth, and Environmental Sciences, Faculty of Environment, University of Northern British Columbia, 333 University Way, BC V2N 4Z9, Prince George, Canada.
Email: raquel.portes@unbc.ca

Present address

Raquel Portes, Department of Geography, Earth, and Environmental Sciences, Faculty of Environment, University of Northern British Columbia, Prince George, Canada.

Assigned to Associate Editor Caitlin Hodges.

Abstract

Quantifying soil redistribution rates, including both erosion and deposition, is critical for understanding erosion processes, landscape evolution, land management strategies, and the carbon cycle. In the Northeast Pacific coastal temperate rainforest, the interaction of perhumid climate and dense coniferous forest tends to form Spodosols which are soils characterized by a subsurface accumulation of organic matter and iron and aluminum oxides, across a range of contrasting lithologies. Deep Spodosols are frequently found on steep backslopes (up to 60%) of colluvial deposits, where shallower soils would typically be expected. We hypothesized that deep Spodosols in Southeast Alaska indicate slope stability, exhibiting negligible soil redistribution rates and stable surfaces regardless of the lithology. Our objective was to quantify soil redistribution rates for Spodosols formed on steep slopes across a range of lithologies in hilly and mountainous areas of Juneau, AK. We used $^{239+240}$Pu isotopes to quantify soil erosion and deposition rates in Spodosols formed on colluvial deposits from tonalite, slate, metavolcanic rock, and phyllite. $^{239+240}$Pu measurements revealed negligible soil redistribution rates for all studied pedons, ranging

Abbreviations: CIS, Cordilleran Ice Sheet; FRNs, fallout radionuclides; LGM, Last Glacial Maximum; NPCTR, Northeast Pacific coastal temperate rainforest; PDM, Profile Distribution Model; SOC, soil organic carbon; UV, uniformity value.

from erosion rates of 0.51 t/ha/year to deposition rates up to 0.43 t/ha/year. No difference was detected between the hill and mountain landforms, further supporting the idea that Spodosols could indicate slope stability over decadal timescales across the region. Understanding the resilience of Spodosols to erosion processes in varied lithologies and landforms on steep slopes is paramount for making informed decisions regarding sustainable land use, landslide risk mitigation, and effective carbon sequestration strategies.

1 | INTRODUCTION

The assessment of soil redistribution rates, including both erosion and deposition, is crucial for understanding soil erosion processes and their effects on carbon storage, water quality, and human safety. Soil redistribution processes in hilly and mountainous terrains can lead to the loss of soil organic carbon (SOC), impacting its long-term persistence in soils (Hunter et al., 2024). Soil erosion and deposition can also influence water quality in streams by introducing sediments and nutrients, potentially triggering cascading effects on aquatic ecosystems and water resources (Owens, 2020). Moreover, erosion processes can pose hazards to human settlements and infrastructure through an increased risk of landslide (Pudasaini & Krautblatter, 2021).

Most soil redistribution studies have focused on the impact of land-use change in agricultural landscapes (Calitri et al., 2019; Lal et al., 2013; Quine & Walling, 1991; Velasco et al., 2018; Wilken et al., 2020, 2021; Zhang et al., 1990), while fewer have explored the relationship between soil development and soil redistribution rates in natural environments (Musso et al., 2020; Portes et al., 2018; Raab et al., 2018; Šamonil et al., 2019; Zollinger et al., 2015). These studies have focused on the effects of time (Musso et al., 2020; Portes et al., 2018; Wilken et al., 2021), climate (Raab et al., 2018; Zollinger et al., 2015), and vegetation (Šamonil et al., 2019) on soil development and soil erosion rates. However, studies integrating lithologic and topographic effects on soil formation and erosion processes remain scarce (e.g., Musso et al., 2020).

Lithology plays a pivotal role in shaping soil properties, which can have a strong influence on soil erodibility. Soil properties such as depth, texture, structure, porosity, organic matter content, and permeability are governed by the diversity of minerals present in the rocks, each possessing different weathering rates. These varying rates of weathering influence the evolution of soil profiles, thereby affecting the resistance of soils to erosion processes (Lal & Elliot, 1994).

Landforms affect drainage and sediment fluxes that influence soil development and erosion processes (Schaetzl & Anderson, 2005). For example, slope position contributes to the variability of soil erosion and deposition rates along hillslopes. Soils located on shoulder, which is the upper part of the slope immediately below the summit, have the greatest potential for erosion by runoff due to slope steepness and tend to be shallow and weakly developed (King et al., 1983). The backslopes are transportational slopes positioned between the erosion-prone upper slopes and the sediment-accumulating lower slopes or footslopes. Several studies have demonstrated higher erosion rates in backslope positions due to the movement of debris and water in diverse environments (Bouhlassa & Bouhsane, 2023; Chen et al., 2022; Li et al., 2019; Martz, 1992). Slope gradient controls the potential energy of a slope, influencing water runoff and infiltration. Steeper slopes are more likely to generate runoff and cause detachment of sediment from the slopes (Huggett, 1975). Slope length is also related to erosion potential; increasing slope length leads to water accumulation and faster runoff (Liu et al., 2000). Building on the established knowledge that slope position and gradient are critical in controlling erosion processes, this study focus on backslopes positions across the landscape of Southeast Alaska, a mountainous region with diverse lithologies. Backslopes are key area of concern for soil loss due to their inherent steepness and associated increased runoff. By focusing on these specific slopes, we aim to deepen our understanding of the effects of lithology and topography on soil redistribution rates.

Southeast Alaska, located within the Northeast Pacific coastal temperate rainforest (NPCTR), is notable for its carbon-rich Spodosols (McNicol et al., 2019; Spinola et al., 2022). Spodosols in this region are deep, often exceeding 100 cm, and formed from a wide range of lithologies (Heilman & Gass, 1974; Spinola et al., 2022). These soils are found on steep mid-backslope positions in both hill and mountain landforms (D'Amore et al., 2012, 2015; Spinola et al., 2022; USDA, 1996). The combination of the perhumid climate and dense coniferous forest tends to overprint the influence of lithology on soil properties (Heilman & Gass, 1974; Spinola et al., 2022). In this region, soil distribution follows a relatively predictable pattern where Spodosols formed from well-drained colluvial deposits occupy upland landscapes across different lithologies. Lower backslope positions often have Spodosols with aquic moisture regimes, while Histosols develop from poorly drained parent materials and are typically found in footslope and toe slope positions (D'Amore et al., 2012, 2015). As a result, Spodosols in this region exhibit a relatively consistent set of characteristics, including a sequence of O, E, Bh, Bhs, and Bs horizons, thick spodic horizons that typically range between 20 and 40 cm, and andic properties (Heilman & Gass, 1974; Spinola et al., 2022). Combined, these characteristics underscore the maturity of Spodosols in the region and could indicate relative slope stability and low erosion and deposition rates. The occurrence of Spodosols on steep hillslopes has also been observed elsewhere across the NPCTR, such as in British Columbia where Spodosols are the predominant soil order (Carpenter et al., 2014). Therefore, the quantification of soil redistribution rates in Southeast Alaska is instrumental in elucidating the role of lithology and associated landforms on soil development and slope stability across the NPCTR region.

Fallout radionuclides (FRNs) such as ^{137}Cs and $^{239+240}$Pu isotopes allow the tracking of soil particles over decadal timescales (≈60 years), offering insights into soil erosion and deposition processes (Alewell et al., 2017; FAO/IAEA, 2017; Zhang et al., 1990). Recently, $^{239+240}$Pu isotopes have emerged as effective tools for estimating soil redistribution rates (Alewell et al., 2017; Calitri et al., 2019; Meusburger et al., 2016, 2018; Musso et al., 2020; Portes et al., 2018; Raab et al., 2018; Schimmack et al., 2001; Wilken et al., 2020; Xu et al., 2013; Zollinger et al., 2015). Compared to other soil erosion tracers (e.g., ^{137}Cs and ^{210}Pb), Pu isotopes have attracted increased attention recently because of their longer half-life, low cost of measurement, and more uniform distribution in mountain environments (Alewell et al., 2014; Meusburger et al., 2016; Zollinger et al., 2015). Consequently, Pu isotopes have proven to be a robust tracer for quantifying decadal soil redistribution rates.

$^{239+240}$Pu isotopes are anthropogenic radionuclides that were emitted to the atmosphere mainly by nuclear weapons tests during the 1950s–1960s. Once deposited on the soil surface, they strongly bind to soil colloids such as organic matter and iron and aluminum oxides and their removal is associated with soil erosion processes (Ketterer et al., 2011). Over time, Pu isotopes are redistributed across the landscape together with soil particles by erosion and deposition processes where eroded sites become depleted in Pu isotopes, whereas depositional sites become enriched. Undisturbed sites, free from soil redistribution dynamics, are assumed to maintain their original fallout $^{239+240}$Pu input, reduced only by radioactive decay, and can serve as reference sites (Alewell et al., 2017; FAO/IAEA, 2017). The undisturbed reference site can then be compared with Pu isotope activity at a soil location to determine the enrichment or depletion of Pu isotopes, thereby indicating the removal or addition of soil material. Using this technique, we can estimate soil redistribution rates over roughly 60 years, from the peak of Pu isotopes deposition in 1963 to the day of soil sampling (Walling & Quine, 1990; Zhang et al., 1990).

Core Ideas

- Deep Spodosols are formed on steep backslopes in rainforests of Southeast Alaska.
- Decadal soil erosion and deposition rates were quantified across varied lithologies.
- Calculated $^{239+240}$Pu soil erosion and deposition rates are negligible.
- Spodosols are in a near stable condition in terms of recent soil erosion processes.

In this study, our objective was to quantitatively assess soil erosion and soil deposition rates in Southeast Alaska using $^{239+240}$Pu. We hypothesized that deep Spodosols formed from different lithologies on backslopes in Southeast Alaska exhibit negligible soil redistribution rates, thus presenting stable surfaces on a decadal time scale. We expect that our results will shed light on the influence of lithology and landform on soil erosion processes within temperate forested environments. Such insights are invaluable as they can inform forest management practices, contribute to more accurate landslide risk assessments, and enhance a better understanding of the carbon cycle.

2 | MATERIALS AND METHODS

2.1 | Study sites

The study area is located in the vicinity of Juneau, AK, which is part of the Northeast Pacific Coastal temperate rainforest (NPCTR), the largest temperate rainforest in the world, extending from California to Southeast Alaska (Figure 1). The climate, as observed from 1971 to 2000 by the NOOA (2020), is wet-maritime with persistent and abundant precipitation (mean annual precipitation of 1400 and 2400 mm as snowfall), no seasonal drought, and a mean average temperature of 4.7˚C at sea level.

The major tree species in the study location are western hemlock (*Tsuga heterophylla*) and Sitka spruce (*Picea sitchensis*) with occasional presence of mountain hemlock (*Tsuga mertensiana*) at high elevations along with red alder (*Alnus rubra*) and Sitka alder (*Alnus viridis* ssp. *sinuata*) in disturbed patches. The forest understory is dominated by blueberry (*Vaccinium ovalifolium*) and devil's club (*Oplopanox horridus*), and the forest floor is generally covered by a carpet of moss, comprised mostly of Rhytidiadelphus and *Hylocomium* ssp. (Heilman & Gass, 1974).

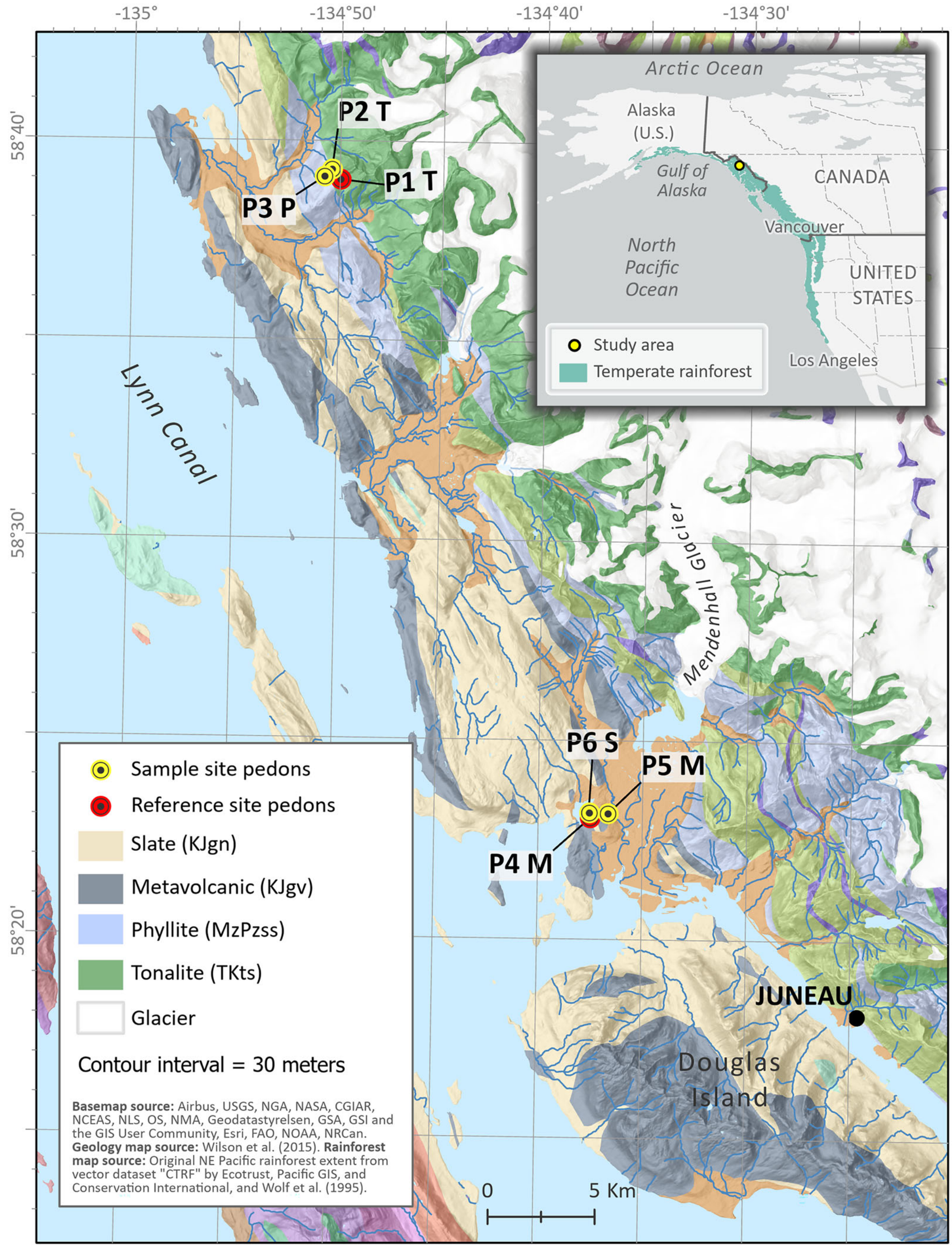

FIGURE 1 Location of the study area in Juneau, Southeast Alaska, within the coastal temperate rainforest of North America. It includes a detailed geological map of the sampling locations. Yellow circles represent the study sites, and red circles indicate the reference sites. Pedon/Site: P = Pedon, T = Tonalite, P = Phyllite, M = Mafic metavolcanic, S = Slate.

The landscape of Southeast Alaska was formed through the accretion of geologic terranes (Figure 1) due to the subduction of the Pacific plate under the North American continent and includes sedimentary, igneous, volcanic, and metamorphic rocks ranging in age from Triassic to Paleocene (Gehrels & Berg, 1992; Miller, 1975). Glacial periods have created a landscape with wide U-shaped valleys, deep fjords, and jagged and rounded mountain summits. Unconsolidated Quaternary deposits cover the postglacial landscape of Southeast Alaska. These deposits include glacial sediments from the Last Glacial Maximum (LGM), uplifted glaciomarine deposits influenced by glacial rebound, alluvial sediments from stream activity, deltaic deposits at the mouths of streams, beach sediments, and colluvial deposits which accumulate due to gravity-driven processes on slopes (USDA, 1996). During the LGM, most of the Southeast Alaska region was covered by the Cordilleran Ice Sheet (CIS) (Carrara et al., 2007; Lesnek et al., 2018). Recent ^{10}Be surface exposure ages of the region indicate that the earliest retreat of the CIS occurred ∼15 ka, but persisted until ∼11 ka due to the remaining local glaciers on the high summits and cirque floors (Lesnek et al., 2020).

The complex geology of the region includes accreted terranes characterized by diverse rock types. Tonalite and phyllite are commonly found in the mountain landforms, while slate and metavolcanic rocks are associated with hill landforms (Figure 1). Mountain landforms are marked by subalpine, rounded/flat summits that were overridden by the CIS during the LGM (USDA, 1996). Occupying high elevations ranging from 790 to 840 m a.s.l., these landforms display smooth, continuous steep slopes (37%–55%). These slopes, which extend approximately 400 m from the summit to mid-backslope positions, are infrequently dissected by ravines. Furthermore, mountain landforms intercept orographic storm events and transport large volumes of water as runoff from rain and summer snowmelt from the mountain summits (USDA, 1996). Conversely, hill landforms are found at lower elevations, ranging from 90 to 150 m a.s.l. Slopes on the hill landforms are generally convex, ranging from 55% to 60%, and are generally broken hillslopes with continuous or discontinuous benches that transect the side slopes. These slopes extend approximately 150 m from the summit to mid-backslope positions. In contrast to mountain landforms, hill landforms do not receive rainfall runoff or snowmelt from mountain summits and cannot yield large volumes of runoff due to their shorter slopes and smaller areas (USDA, 1996).

Soil formation in this region occurs at some of the fastest rates worldwide, facilitated by a combination of a perhumid climate and dense coniferous forests (Chandler, 1942; Crocker & Dickson, 1957). The high levels of precipitation facilitate extensive chemical weathering, leaching of base cations, and illuviation of organic matter, Al, and Fe to subsurface horizons. Moreover, coniferous forests contribute to soil acidification through the production of organic acids, which speeds up chemical weathering and further accelerating soil formation rates (Alexander & Burt, 1996; Bormann et al., 1995; Chandler, 1942; Crocker & Dickson, 1957). As a result, Spodosols can form on coarse-textured till deposits in Southeast Alaska in under 300 years (Alexander & Burt, 1996; Chandler, 1942), and in fewer than 400 years on sandy beach deposits in coastal British Columbia (Singleton & Lavkulich, 1987).

2.2 | Experimental set-up — Reference and study sites

The quantification of soil redistribution rates takes into account the reduction or enrichment of the $^{239+240}$Pu inventories (total radionuclide activity per unit area) of a "study site" relative to a nearby undisturbed "reference site." Therefore, the enrichment or depletion of Pu isotopes in the study site corresponds to the accumulation or removal of soil particles (Alewell et al., 2014, 2017). To quantify soil redistribution rates in old-growth forests across different lithologies in Southeast Alaska, we selected four study sites in mid-backslope landscape positions in areas composed of tonalite, phyllite, slate, and mafic metavolcanic rocks (Figure 1). These sites are representative of the broader landscape features of the region, including the occurrence of deep Spodosols that are common on steep mid-backslope positions across the diverse lithologies. Sites representing tonalite and phyllite rocks are located within the Héen Latinee Experimental Forest, north of Juneau, while those representing slate and mafic metavolcanic are located to the south, within the Auke Lake and Montana Creek watersheds, respectively (Figure 1). All study sites share a northerly aspect, ranging from 325˚N to 10˚N, with a convex slope shape and inclinations varying between 37% and 60% (Table 1). These study site locations are the same as those previously studied by Spinola et al. (2022) who verified the colluvial origin of the sediments via in-depth field inspections, petrographic descriptions, and mineralogical composition analyses. Sites with similar characteristics were intentionally selected to ensure meaningful comparisons across all study sites.

For our reference sites, we selected two areas located at the summit above the study slopes, one composed of tonalite in the Héen Latinee Experimental Forest and the other of metavolcanic rocks in the Montana Creek Watershed (Figure 1). The selection of reference sites followed the protocols outlined by FAO/IAEA (2017). Specifically, we carefully chose undisturbed, flat areas situated at the summit of slopes with no visible signs of disturbance to ensure that soil erosion and deposition processes were minimal since the deposition of Pu isotopes. We accounted for the pit and mound microtopography, as these sites were free from the soil disturbances typically associated with recent tree throw events. Additionally, we used the degree of soil development as a relative age marker to select undisturbed sites, given that tree throw events can disrupt soil horizons and soil redistribution processes (Bowers, 1987). In Southeast Alaska, buried or broken organic and Bhs horizons are not visible in the Spodosols after 350 years due to fast pedogenesis rates (Bormann et al., 1995). Therefore, our reference sites were pedons with O, E, and Bhs horizons that showed no signs of horizon disturbance.

2.3 | Pedon description and sampling

A total of six pedons were described and sampled, one at each of the four study sites and two reference sites. Soil pits were excavated to the C or Cr horizons, and approximately 500 g of soil (bulk samples) was taken for each soil horizon. For bulk density determination, two replicates of undisturbed samples

TABLE 1 Characteristics of the reference and study sites.

Site/pedon	Parent material	Site type	Elevation (m a.s.l.)	Latitude/longitude (°N/°E)	Slope aspect (°N)	Slope (%)	Slope length (m)	Slope position	Slope shape	Vegetation
P1 T	Tonalite	Reference	840	58.65095/−134.8327	340	2	–	Summit	Flat	Mountain hemlock, western hemlock, blueberry, mosses
P2 T	Tonalite	Study	610	58.65511/−134.8398	340	37	≈400	Backslope	Convex/convex	Mountain hemlock, western hemlock, blueberry, mosses, lilies, ferns
P3 P	Phyllite	Study	630	58.65214/−134.8457	325	55	≈400	Backslope	Convex/convex	Mountain hemlock western hemlock, blueberry, mosses
P4 M	Mafic metavolcanic	Reference	150	58.38475/−134.6251	350	2	–	Summit	Flat	Western hemlock, Sitka spruce, blueberry, mosses
P5 M	Mafic metavolcanic	Study	90	58.38660/−134.6107	350	60	≈150	Backslope	Convex/convex	Western hemlock, Sitka spruce, blueberry, mosses
P6 S	Slate	Study	90	58.38681/−134.6257	10	55	≈150	Backslope	Convex/convex	Western hemlock, Sitka spruce, blueberry, mosses

Note: Pedon/Site: P = Pedon, T = Tonalite, P = Phyllite, M = Mafic metavolcanic, S = Slate.

were collected from each soil horizon of the pedons using a cylindrical volumetric core with a volume of 138.5 cm^3. Rock fragments (particles >2 mm) were visually estimated in the field. Pedon descriptions were done following the USDA–NRCS protocols (Schoeneberger et al., 2012) and classified according to the Keys to Soil Taxonomy (Soil Survey Staff, 2014a). We added suffixes T, P, S, and M to each pedon number to represent the lithology: T for tonalite, P for phyllite, S for slate, and M for metavolcanic (Figure 1).

For the assessment of soil redistribution using $^{239+240}Pu$, we collected four replicate samples at each reference and study site. Using a soil corer, undisturbed samples were taken at 5 cm increments from a depth of 0–30 cm. We sampled four experimental sites, two reference sites, four replicates at each = 24 pits × 6 depth intervals = 144 soil core samples. These soil core samples were also used to determine bulk densities for Pu activity calculation. To minimize spatial variability, the replicate locations were carefully selected to be approximately 2–5 m apart from the described pedon and were aligned along contour lines, ensuring a consistent slope shape and length across sampling locations.

To assess soil redistribution rates for the tonalite and phyllite study sites, we used the Pu inventories collected at the tonalite reference site. Conversely, for the slate and mafic metavolcanic study sites, we used the Pu inventories from the metavolcanic reference site (Table 1). To ensure accurate comparisons between reference and study sites, we adhered to the site selection protocols suggested by FAO/IAEA (2017) and IAEA (2014), which emphasize the importance of maintaining consistency in environmental factors. Recognizing that the fallout of Pu isotopes at a location is influenced by a variety of environmental factors, including climate, microclimate, vegetation, altitude, and latitude (Meusburger et al., 2020), we strategically selected our reference and study sites to be less than 1 km apart. This proximity was intentionally chosen to guarantee the consistency of these factors across the sites, therefore guaranteeing that all sites received a similar deposition of Pu isotopes.

2.4 | Soil sample preparation and lab analyses

Bulk samples from soil horizons, along with bulk density and soil core samples from the depth increments, were oven-dried at 70°C for 48 h and sieved to <2 mm to obtain fine-earth fraction. We calculated the bulk density (g/cm^3) according to Soil Survey Staff (2014b) guidelines by dividing the dry weight of the soil core (<2 mm) by the volume of the soil core. Rock fragments were excluded from the calculation. The core samples were ground to a fine powder (≈60 μm) for soil organic carbon (SOC), and $^{239+240}Pu$ measurements. Soil pH was determined using a 1:2.5 soil:water solution ratio. Particle size distribution was determined by sieving for sand fractions and pipette method for silt and clay (Gee & Bauder, 1986; Soil Survey Staff, 2014b). Sand fractions included very fine sand (100–50 µm), fine sand (250–100 µm), medium sand (500–250 µm), coarse sand (1000–500 µm), and very coarse sand (2000–1000 µm). The total sand content was obtained by summing these fractions. Before particle size analyses, organic matter was removed using a 10% hydrogen peroxide solution (Mikutta et al., 2005). The SOC content was measured using a continuous-flow isotope ratio mass spectrometer. The method uses a Thermo Scientific Flash 2000 elemental analyzer and a Thermo Scientific Conflo IV interfaced with a Thermo Scientific Delta V Plus mass spectrometer. Quality controls were measured in every 10 samples. The instrumental standard deviation was 0.68%. The analyses were conducted at the Alaska Stable Isotope Facility, University of Alaska Fairbanks.

We quantified Fe and Al in the fine earth fraction (<2 mm) using an ammonium oxalate solution (0.2 M, pH 3) (Schwertmann, 1964) to extract organometallic complexes and short-range-ordered Fe and Al hydroxides (Fe_o and Al_o). The extracts were measured using a microwave plasma-atomic emission spectrometer (Agilent 4200 MP-AES). The data were used to calculate the Al_o + ½ Fe_o ratio which is a taxonomic criterion for andic soil properties. Values ≥ 2% are indicative of andic properties (Soil Survey Staff, 2014a). This analysis was conducted for soil classification and maturity evaluation purposes. Lithologic discontinuities were identified based on the uniformity of the parent material along the depth profile, using the percentage of rock fragments and the uniformity value (UV) index (Cremeens & Mokma, 1986; Portes et al., 2016; Schaetzl, 1998). The UV index compares particle size fractions from upper and lower contiguous horizons (Equation 1). UV values closer to 0 indicate similarity to the parent material of the two contiguous horizons, and values exceeding ±0.6 suggest a potential lithologic discontinuity (Cremeens & Mokma, 1986). Because the soils were developed on colluvial deposits, the identification of lithologic discontinuities provided additional information regarding their erosional/depositional history at each site.

$$\text{UV index} = \frac{\frac{(\%\text{silt}+\%\text{very fine sand})}{(\%\text{sand}-\%\text{very fine sand})} \text{ in the upper horizon}}{\frac{(\%\text{silt}+\%\text{very fine sand})}{(\%\text{sand}-\%\text{very fine sand})} \text{ in the lower horizon}} - 1 \tag{1}$$

2.5 | Sample preparation and measurement for $^{239+240}$Pu activities

Sample preparation and measurement for $^{239+240}$Pu activities were performed according to Ketterer et al. (2004). Five grams of milled soil core samples were dry-ashed for 20 h at 600°C in 40 mL Pyrex vials to remove organic matter. Some samples with high organic matter content showed refractory carbon after the dry-ashing step and required an additional dry-ashing to complete combustion. A spike of ca. 49.4 pg (0.08466 Bq/g) of ^{242}Pu tracer solution (NIST 4334) was added to the sample vials. The samples were then leached using 10 mL of 16 M HNO_3 in a heating oven for 20 h. After acid leaching, deionized water was added to adjust the acidity to ∼8 M HNO_3, the sample-solid suspensions were filtered using 47-mm-diameter 0.45-µm cellulose nitrate membranes, and the filter cakes were rinsed with small amounts of additional water to achieve volumes of ∼25 mL and ∼6 M HNO_3 concentration. The filtered solutions were transferred to 50 mL polypropylene centrifuge tubes; Pu species were adjusted to a Pu^{4+} oxidation state using an acidified $FeSO_4.7H_2O$ solution (2 mg/mL of leached solution) and $NaNO_2$ solution (20 mg/mL of solution). The Fe^{2+} solution was added first and subsequently, the sodium nitrite solution was added. The addition of $NaNO_2$ (aq) to HNO_3 solutions produces toxic NO_2 (g), which must be vented in a suitable fume hood. Thereafter, the samples were heated at 75°C, and uncapped for 2 h in a vented convection oven. After cooling, 100 mg of TEVA resin (ElChrom) was added to each sample and shaken using a horizontal shaker for 2 h so that the TEVA uptakes the tetravalent Pu. Thereafter, the resin was collected using a 23-mL "jumbo" polyethylene transfer pipette containing a glass wool plug. The resin columns thus formed were rinsed to remove contaminant actinides (i.e., U and Th) using acid solutions in the following sequence: 16 mL of 2 M HNO_3; 10 mL of 8 M HCl, and 6 mL of 2 M HNO_3. Pu was eluted from the sample columns into microcentrifuge tubes using the following sequence: (i) 0.4 mL H_2O, (ii) 0.4 mL of 0.05 M ammonium oxalate, and (iii) 0.4 mL H_2O. The resulting solution was directly analyzed without any further dilution or evaporation/reconstitution.

Data quality was evaluated using control samples: five "negative controls" (Pu-devoid sandstone) to serve as blanks; three Certified Reference Material IAEA-384 (Fangataufa lagoon sediment), seven reagent-only blanks, and 25 replicates of individual soil samples. The measurements of Pu isotopes were conducted using a Thermo X Series II quadrupole inductively coupled plasma-mass spectrometry equipped with a high-efficiency desolvating nebulizer system APEX HF at Northern Arizona University. The 235, 238, 239, 240, and 242 masses were measured; the extent of mass discrimination was corrected using a mass bias factor determined from measurements of $^{235}U/^{238}U$ for a natural U solution (0.00725 in nature). A $^{238}U^1H^+/^{238}U^+$ correction factor was determined using a ^{238}U solution, and the resulting factor was used to subtract small isobaric contributions of $^{238}U^1H^+$ to signals observed at m/z 239. The $^{240}Pu/^{239}Pu$ atom ratio was determined to ascertain the source(s) of Pu contamination, for example, global versus regional fallout sources from

Chernobyl or the Nevada Test Site (Ketterer et al., 2004). The source of Pu contamination is critical as it influences the total $^{239+240}$Pu inventories, serving as an additional approach to evaluate the suitability of reference sites. The masses of ^{239}Pu and ^{240}Pu were determined relative to the known mass of ^{242}Pu tracer, and subsequently converted into activity concentrations (Bq/kg) and expressed as a summed $^{239+240}$Pu activities.

2.6 | Determination of $^{239+240}$Pu inventories and conversion into soil redistribution rates

We determined the total soil $^{239+240}$Pu inventories (Bq/m^2) using the following equation:

$$A(s) = \frac{1}{S} \sum_i M_{Ti} C_i \tag{2}$$

where $A(s)$ is the $^{239+240}$Pu inventories (Bq/m^2), S is the cross-sectional area of the soil core (m^2), M_{Ti} is the total mass of the ith sample depth increment (kg), and Ci is the activity of the ith subsample depth increment (Bq/kg).

We used the Profile Distribution Model (PDM) (Equation 3) according to Walling and Quine (1990) and Zhang et al. (1990) to convert $^{239+240}$Pu inventories into soil redistribution rates:

$$A\prime\,(x) = A_{\mathrm{ref}}\left(1 - e^{\frac{x}{h_0}}\right) \tag{3}$$

where $A\prime(x)$ is the amount of isotope inventory above depth x (Bq/m^2), x is the depth from the soil surface expressed as the mass between the top and actual depth (kg/m^2), A_{ref} is the reference inventory, expressed as a mean of all reference sites (Bq/m^2), and h_0 is the profile shape factor (kg/m^2) that describes the rate of exponential decrease in inventory with depth for soil profiles in reference sites. We excluded the 0–5 cm increment of the mafic metavolcanic reference and study sites because those samples were mostly fresh plant debris and not part of the O horizon. We calculated soil redistribution rates based on a comparison of $^{239+240}$Pu isotopes inventories from the study and reference sites.

The soil redistribution rate Y was calculated according to Walling and He (1999) and Zhang et al. (1990):

$$Y = \frac{10}{t - t_0} \times \ln\left(1 - \frac{X}{100}\right) \times h_0 \tag{4}$$

where Y is erosion or deposition rate (t/ha/year), t is the year of sampling (i.e., 2019), t_0 is a reference year for thermonuclear weapon testing (i.e., 1963—global fallout peak) commonly used for $^{239+240}$Pu analyses, and X is % reduction or increase in total inventory (A_u [Bq/m^2]) in relation to the reference site value [$(A_{\mathrm{ref}} - A_u)/A_{\mathrm{ref}} \times 100$]. The uncertainties for the $^{239+240}$Pu total inventories at the reference and study sites, as well as for the soil redistribution rates, are reported as 1-sigma standard error (SE). This was calculated for each dataset by dividing the standard deviation by the square root of the number of replicates, which is four for all reference and study sites.

3 | RESULTS

3.1 | Soil morphological, physical, and chemical characteristics

All pedons show a typical horizon sequence for Spodosols with O, E, Bh, Bhs, and/or Bs, C horizons (Figure 2; Table 2). Soil depth at reference sites was shallower compared to study sites. At reference sites, soil depths were 45 and 50 cm for P1 T and P4 M pedons, respectively. Soil depths were more heterogeneous in study sites; P5 M was the deepest with 158 cm, followed by P6 S (140 cm), P2 T (110 cm), and P3 P (87 cm). The thickness of O horizons was similar across all pedons, including reference and study sites, ranging from 3 to 15 cm. Only P1 T at the study site had a thinner O horizon, with 3 cm. They are composed mainly of mosses, fibers, and weak to moderately decomposed plant materials. Organic horizon bulk densities ranged from 0.05 to 0.23 g/cm^3.

Likewise, E horizons were also consistent across the pedons, averaging 5 cm thick. Spodic horizons (i.e., the combination of Bh, Bhs, and Bs) were thinner at reference sites than at study sites. At reference sites, the thickness of the spodic horizons was 32 cm for tonalite and 29 cm for the metavolcanic pedon. The thickness of spodic horizons at study sites ranged from 91 cm in P5 M, 76 cm in P6 S, 72 cm in P2 T, and 37 cm in the P3 P pedon. The bulk density of mineral horizons, including E, B, and C horizons, ranged from 0.23 to 0.84 g/cm^3.

All pedons shared similar trends in terms of pH, SOC contents, and structure. The pH was acidic, ranging between 3.7 and 5.7, and increasing with depth. SOC contents were very high in the O horizons, ranging from 359.2 to 473.5 g/kg. The SOC contents in the spodic horizons were relatively high, ranging from 13.5 to 152.5 g/kg (Table 2). All pedons showed an abundance of very fine to very coarse roots that are concentrated mostly in the upper horizons (up to ≈25 cm deep).

All pedons met the requirements for the Spodosol order and the Cryic suborder (Soil Survey Staff, 2014a). P1 T and P6 S meet the requirements for the Humic great group, which is defined by organic carbon content >6% for at least 10 cm of the spodic horizons. The other pedons are Haplic. Except for P1 T and P2 T, all pedons have andic soil properties, as evidenced by values higher than 2% for the Al_o + ½ Fe_o ratio in

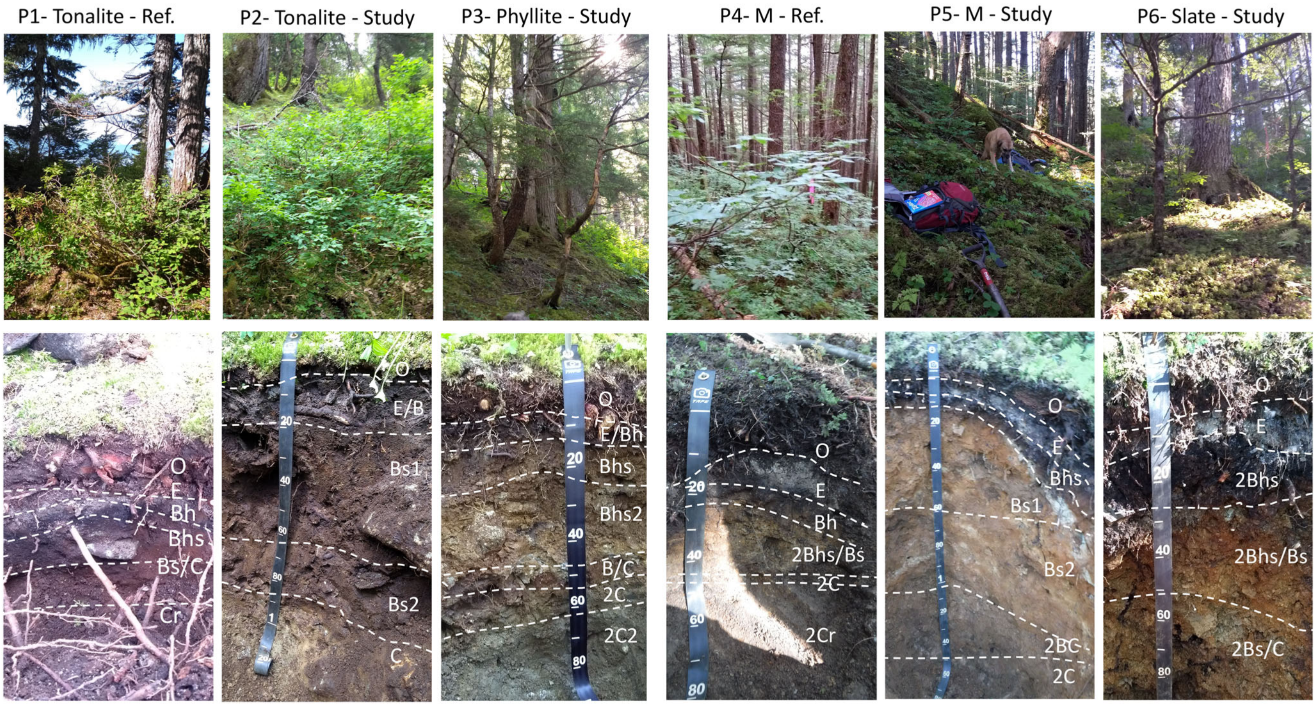

FIGURE 2 Typical terrain of the reference and study sites (upper) and the sampled pedons (lower). Dashed lines in the sampled pedons represent the soil horizon boundaries. The pedons selected as reference and study sites show a general sequence of O, E, Bhs, Bs, and C horizons.

the B horizons, low bulk density ($\leq$0.90 g/cm^3), and meeting the thickness requirements for the Andic subgroup (Table 2).

At the study sites P2 T and P3 P, the soil parent material comprises tonalite and phyllite colluvial deposits, respectively, with angular rock fragments overlying compact glacial till. In contrast, the soil parent materials at the study sites P5 M and P6 S consist of colluvial deposits of mafic metavolcanic and slate, respectively. The reference site P1 T is primarily composed of glacial till, consisting of rounded pebbles, cobbles, and boulders, with a predominant tonalite composition, along with a minor proportion of mafic rocks. Meanwhile, the P4 M reference site was formed from mafic metavolcanic sediments.

Lithology had some influence on particle size distribution. Metavolcanic and slate pedons were finer, with silt loam to loam textures, tonalite pedons were coarser showing sandy loam to loamy sand texture and phyllite pedons had a more widespread distribution, ranging from silt loam to loamy sand. No differences in texture were noticed between the reference and study sites. Overall, all pedons had a high percentage of rock fragments ($\geq$2 mm), ranging from 15% to 70% (Table 2). Lithologic discontinuities were identified in all pedons, except P2 T. Some discontinuities were detected in the field while others were identified using the UV index (Table 2). In the field, abrupt textural change and/or abrupt presence/absence of large rock fragments were the most striking feature used to recognize a discontinuity. Although lithologic discontinuities indicative of different depositional periods were observed within the soil profiles, the lithology, from which these layers were derived remained consistent across the varying strata.

3.2 | ^{240}Pu/^{239}Pu atom ratio and $^{239+240}$Pu inventories

The average ^{240}Pu/^{239}Pu atom ratio for all samples from the reference and study sites measured 0.18 ± 0.005 (Figure 3). Similar average values of the ^{240}Pu/^{239}Pu ratio were found for all depth increments. Of note are the scattered values at greate depths. This is primarily due to an artifact of the analytical procedure. As the soil depth increases, the Pu activities decrease, leading to fewer ion counts at m/240 of the deeper intervals. Consequently, the measured ratios are constrained by weak signals in the soil.

The $^{239+240}$Pu inventories of all reference and study sites exhibit a similar depth distribution, where most of the Pu isotope inventory (75%–89%) is concentrated at the soil surface (0–15 cm) and inventory decreases exponentially with depth (Figure 4). The total $^{239+240}$Pu inventories were also similar for the reference and the study sites for both hill and mountain landforms. For the mountain landform, the tonalite reference and study sites exhibit similar values: 103.4 ± 14.7 Bq/m^2 and 103.8 ± 13.4 Bq/m^2, respectively. A slightly higher value was found for the phyllite study site (130.9 ± 12.6 Bq/m^2). For the hill landform, almost identical values were found for the mafic metavolcanic reference and study sites (126.2 ± 14.9 Bq/m^2

TABLE 2 Soil morphological, physical, and chemical properties of the investigated pedons.

Site/pedon					Particle size distribution								Soil structure			Roots	
Horizon	Depth (cm)	Munsell color (moist)	BD (g/cm³)	RF (%)	Sand[a] (%)	VFS[b] (%)	Silt[c] (%)	Clay[d] (%)	Texture[e]	UV index[f]	SOC (g/kg)	pH[g]	Grade[h]	Type[i]	Size[j]	Q[k]/S[l]	Al_o + ½ Fe_o[m] (%)
P1 T (reference site)—Lithic Humicryod																	
O	0–9	7.5YR 3/2	0.23	–	–	–	–	–	–	–	380.5	4.1	–	–	–	2/M, 2/F, 1/VC	–
E	9–13	10YR 6/1	0.53	1	74.2	13.5	22.0	3.9	LS	0.15	32.4	4	1	SBK	F	1/M, 1/F	0.4
Bh	13–18	10YR 2/1	0.80	6	76.7	13.8	18.4	4.9	LS	−0.02	65.3	4.6	2	GR	M	1/M	1.7
Bhs	18–35	10YR 2/1	0.65	30	70.8	12.2	18.4	10.8	SL	−0.31	67.4	4.9	2	SBK	M	1/M	2.2
Bs/C	35–45	5YR 2.5/2	–	30	69.7	14.5	26.9	3.5	SL	–	30.6	5.1	2	SBK	M	–	1.5
Cr	45+	–	–	–	–	–	–	–	–	–	0.4	–	–	–	–	–	–
P2 T (study site)—Typic Haplocryod																	
O	0–3	7.5YR 3/3	0.17	–	0.0	–	–	–	–	–	411.4	4.5	2	SBK	M	2/F, 2/M	–
E/B	3–18	7.5YR 4/2	0.78	60	71.9	12.9	20.5	7.6	SL	0.05	74.5	4.2	2	SBK	M	2/F, 2/M, 1/C	0.5
Bs1	18–63	2.5YR 2.5/2	0.49	70	73.8	12.7	20.5	5.7	SL	−0.02	56.4	4.8	2	SBK	M	1/M	1.8
Bs2	63–90	7.5YR 3/4	0.56	70	70.5	11.4	21.4	8.1	SL	0.22	50.8	5.0	2	SBK	M	–	1.1
C	90–110	10YR 4/6	–	70	77.1	11.7	18.1	4.8	LS	–	9.7	5.2	2	SBK	M	–	0.8
P3 P (study site)—Andic Haplocryod																	
O	0–10	7.5YR 2.5/3	0.20	–	–	–	–	–	–	–	359.2		–	–	–	3/VF, 3/F, 3/M, 3/C	–
E/Bh	10–16	10YR 2/1	0.40	20	–	–	–	–	–	–	191.1	4.2	–	–	–	3/VF	–
Bhs	16–28	10YR 3/3	0.33	45	50.0	7.4	44.5	5.5	L	−0.32	42.8	5.1	1	GR	M	2/F	–
Bhs2	28–47	10YR 4/4	0.33	60	43.6	9.8	50.4	6.0	L	0.26	42.7	5.3	2	SBK	M	2/F	2.1
B/C	47–55	10YR 3/3	–	50	47.9	9.0	46.1	6.0	L	1.38	42.3	5.4	2	SBK	M	–	2.8
2C	55–62	10YR 3/6	–	20	71.9	12.0	23.7	4.5	SL	−0.22	41.2	5.5	2	SBK	M	–	2.3
2C2	62–87	7.5YR 3/4	0.57	20	68.0	14.6	26.4	5.6	SL	−0.40	8.5	5.5	1	SBK	M	–	0.7
2C3	87+	10YR 3/2	–	15	77.0	34.4	19.4	3.6	LS	−0.32	1.7	5.7	0	MA	–	–	0.7
P4 M (reference site)—Andic Haplocryod																	
O	0–14	7.5YR 2.5/2	–	–	–	–	–	–	–	–	458.5	3.7	–	–	–		–
E	14–19	7.5YR 5/3	0.69	5	26.8	13.0	63.6	9.7	SIL	0.69	46.9	4.0	1	SBK	M	3/F, 3/VF, 2/M	0.7
Bh	19–23	7.5YR 2.5/1	0.73	5	32.8	12.7	53.8	13.4	SIL	0.14	29.3	4.5	1	SBK	M	2/F, 2/M, 2/C	2.2
2Bhs/Bs	23–48	7.5YR 3/4	–	50	34.7	10.5	60.0	5.3	SIL	9.37	37.9	4.9	2	SBK	M	–	2.1

(Continues)

TABLE 2 (Continued)

Site/pedon					Particle size distribution								Soil structure			Roots	
Horizon	Depth (cm)	Munsell color (moist)	BD (g/cm^3)	RF (%)	Sand[a] (%)	VFS[b] (%)	Silt[c] (%)	Clay[d] (%)	Texture[e]	UV index[f]	SOC (g/kg)	pH[g]	Grade[h]	Type[i]	Size[j]	Q[k]/S[l]	Al_o + ½ Fe_o[m] (%)
2C	48–50	2.5YR 3/4	–	95	79.2	3.1	18.2	2.6	LS	–	23.2	4.9	0	MA	–	–	1.6
2Cr	50+		–	–						–	0.2	–	–	–	–	–	–
P5 M (study site)—Andic Haplocryod																	
O	0–10	7.5YR 2.5/3	0.12	–	–	–	–	–	–	–	469.8	3.8	–	–	–	3/VF, 3/F, 2/M	–
E	10–14	7.5YR 5/3	0.53	25	30.9	12.4	63.8	5.2	SIL	0.59	34.5	4.1	3	GR	M	2/F, 2/M	0.7
Bhs	14–20	7.5YR 2.5/1	0.58	30	35.5	10.4	54.3	10.2	SIL	0.12	90.1	4.0	2	SBK	M	1/F, 1/M	2.6
Bs1	20–60	5YR 4/6	0.58	40	38.7	10.5	54.2	7.1	SIL	0.47	32.7	5.0	2	SBK	M	–	2.5
Bs2	60–105	5YR 4/6	0.84	45	46.9	9.8	48.4	4.8	SL	0.90	13.5	5.3	2	SBK	M	–	1.8
2BC	105–158	5YR 3/4	–	80	63.4	10.2	33.8	2.8	SL	0.59	4.2	5.5	1	SBK	M	–	1.3
2C	158+	–	–	–	–	–	–	–	–	–	–	–	–	–	–	–	–
P6 S (study site)—Andic Humicryod																	
O	0–10	7.5YR 2.5/3	0.05	–	–	–	–	–	–	–	456.1	5.7	–	–	–	2/F, 1/C, 3/M	–
E	10–16	5YR 6/1	0.25	75	42.9	4.9	50.0	7.1	SIL	0.54	48.7	5.5	0	MA		3/F	0.6
2Bh	16–26	5YR 2.5/2	0.23	15	46.1	3.6	36.3	17.6	L	0.14	152.5	5.5	2	SBK	F	1/C, 1/C	2.7
2Bhs/Bs	26–61	5YR 4/6	0.24	50	51.7	3.3	36.7	11.6	L	0.27	58.0	5.4	1, 2	GR, SBK	VF, VF	1/F, 1/M	2.7
2Bs/C	61–92	7.5YR 5/4	0.19	60	57.8	3.3	32.2	10.0	SL	–	36.8	5.3	–	–	–	–	2.3
2C	92–140+	–	–	70	–	–	–	–	–	–	1.6	5.1	–	–	–	–	–

Abbreviations: BD, bulk density; RF, rock fragments; SOC, soil organic carbon.

[a]Sand = 2000–50 µm.

[b]SVF = Very fine sand = 100–50 µm.

[c]Silt = 50–2 µm.

[d]Clay = <2 µm.

[e]Textural class—LS = Loamy sandy, SL = Sandy loam, SIL = Silt loam, L = Loam.

[f]UV index = Uniformity value index (Cremeens & Mokma, 1986) $\dfrac{\frac{(\%\ \text{silt} + \%\ \text{very fine sand})}{(\%\ \text{sand} - \%\ \text{very fine sand})}\ \text{in the upper horizon}}{\frac{(\%\ \text{silt} + \%\ \text{very fine sand})}{(\%\ \text{sand} - \%\ \text{very fine sand})}\ \text{in the lower horizon}} - 1.$

[g]pH H_2O.

[h]Soil structure—Grade: 0 = Structureless, 1 = Weak, 2 = Moderate, 3 = Strong.

[i]Soil structure—Type: GR = Granular, SBK = Subangular blocky, MA = Massive.

[j]Soil structure—Size: VF = Very fine, V = Fine, M = Medium, C = Coarse.

[k]Roots—Quantity: 1 = Few, 2 = Common, 3 = Many.

[l]Roots—Size: VF = Very fine, F = Fine, M = Medium, C = Coarse, VC = Very coarse.

[m]Al_o + ½ Fe_o: Ammonium oxalate extraction of Fe and Al from pedogenic oxides.

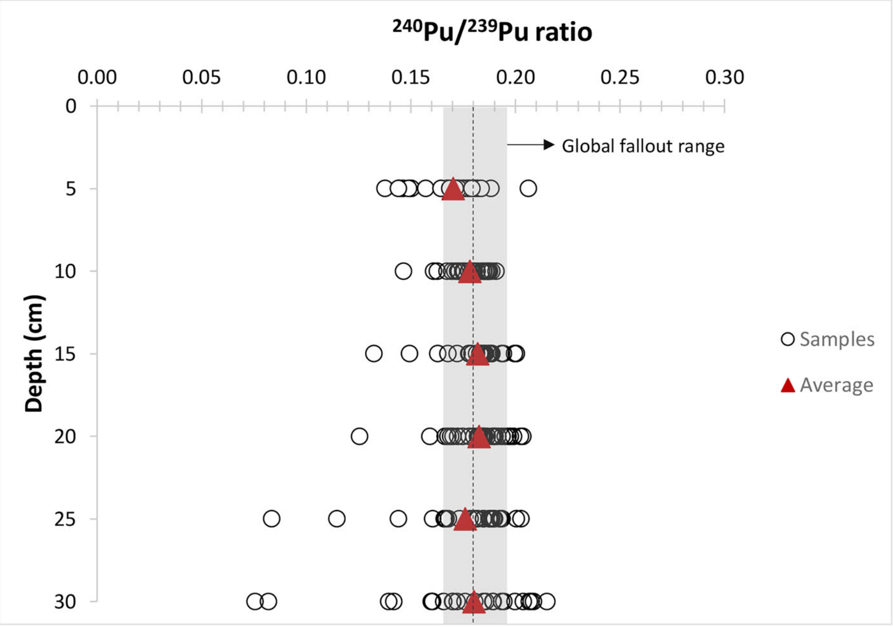

FIGURE 3 $^{240}Pu/^{239}Pu$ atom ratios for all samples (reference and study sites) as a function of sampling depth. The dashed line and gray area indicate the average global fallout value (0.18 ± 0.014) and its range, respectively (Kelley et al., 1999). The average $^{240}Pu/^{239}Pu$ ratio for all our soil samples is 0.18 ± 0.005, which coincides with the global fallout average value.

and 125.5 ± 17.2 Bq/m^2, respectively) and a slightly lower value for the slate study site (115.5 ± 14.4 Bq/m^2; Figure 4).

3.3 | Rates of soil erosion and deposition

All Spodosols across the study sites exhibit similar soil redistribution rates (Figure 5), ranging from 0.43 to −0.51 t/ha/year with negative values indicating erosion and positive values indicating deposition. The standard error is also similar across all study sites, ranging between ±0.90 and 1.16 t/ha/year.

4 | DISCUSSION

4.1 | Spodosol development

All the pedons investigated across our study sites display morphological and chemical characteristics consistent with Spodosols, regardless of lithology and landform. These soils have developed distinct eluvial and illuvial horizons, with relatively thick spodic horizons along with high SOC content, all of which meet the requirements for the Spodosol order (Soil Survey Staff, 2014a). Except for the pedons developed from tonalite, all pedons display andic soil properties, as evidenced by high Al_o + ½ Fe_o ratio values (>2%) in the B horizons, low bulk densities (≤0.90 g/cm^3), and sufficient thickness to meet the Andic subgroup criteria. Although P-retention was not measured in this study, the observed Al_o + ½ Fe_o and bulk density values align well with those found in other Spodosols with andic properties across Southeast Alaska (Alexander et al., 1993; Spinola et al., 2022).

Previous studies in the region have also noted the homogeneous evolution of Spodosols across a wide range of other parent materials, such as granodiorite, phyllite, basalt, volcanic ash, and limestone (Heilman & Gass, 1974; Spinola et al., 2022). The interaction of wet, cool climate and coniferous forest vegetation in Southeast Alaska is optimal for driving podzolization despite the mineral and geochemical composition of the parent material, enhancing (1) acidification of soil solution caused by organic acid compounds that enhance chemical weathering; (2) release of bases, Al, Fe, and Si from soil minerals; (3) leaching of bases and organic compounds; and (4) translocation of Al, Fe, and organic compounds from upper horizons and immobilization in B horizons (DeConinck, 1980; Spinola et al., 2022; Ugolini & Dahlgren., 1987).

The development of Spodosols observed across the study sites is facilitated by various physical characteristics that enhance soil drainage. These features include coarse textures such as silt loam and sandy loam, high content of rock fragments, and dense root systems. The high content of rock fragments (from 15% to 70%) and the moderate/high root density of these coarse-textured Spodosols increased soil porosity and water permeability, facilitating eluvial and illuvial processes to occur (Musielok et al., 2021; Schaetzl, 1991). Moreover, the medium-sized subangular blocky structure and the lack of hydromorphic features also indicate well-drained conditions.

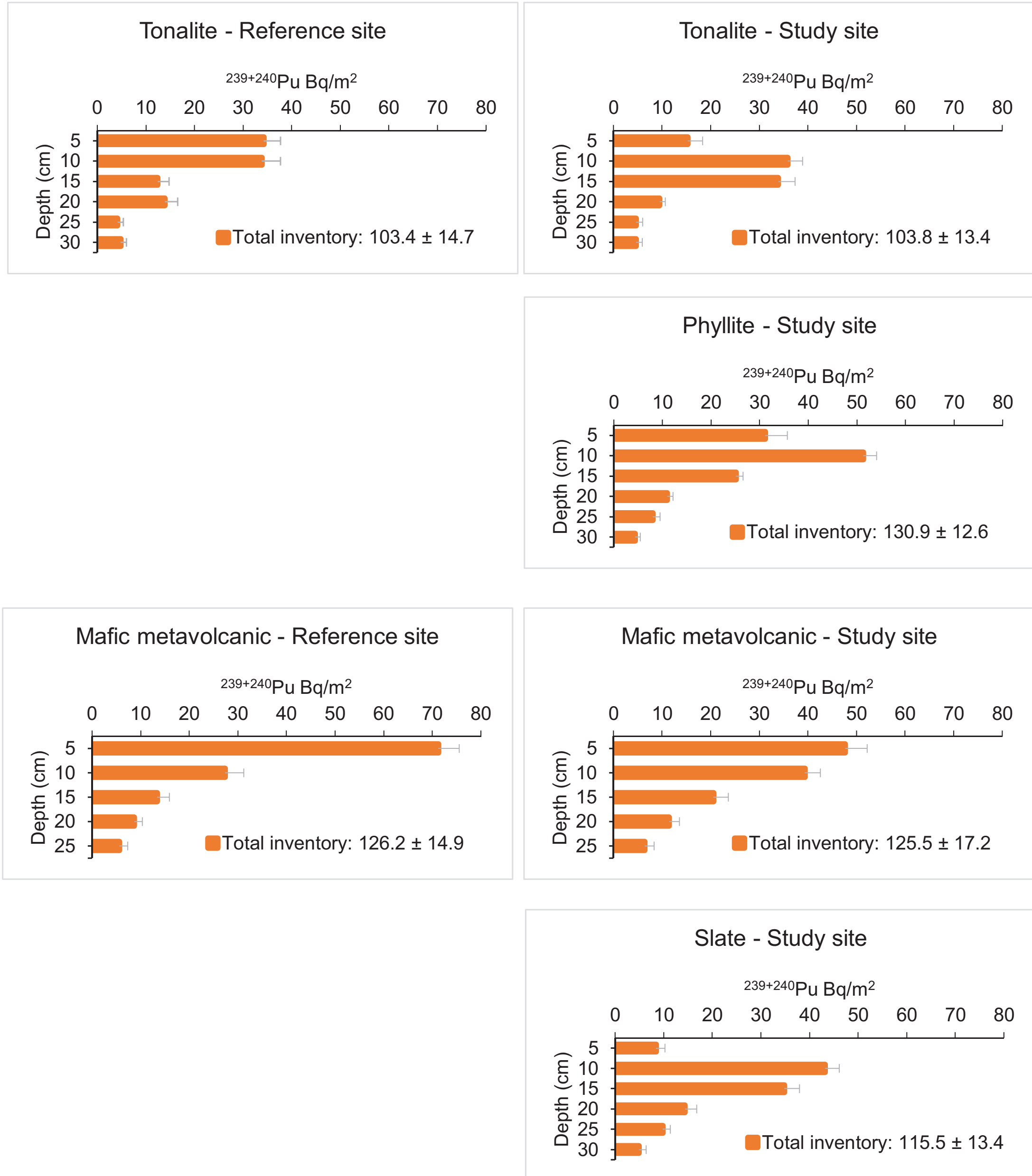

FIGURE 4 Average of the vertical distribution of $^{239+240}$Pu inventory (± standard error) with soil depth and total inventory of the reference and study sites.

The notably low bulk density values observed in the mineral horizons of these Spodosols, ranging from 0.23 to 0.84 g/cm^3, can be attributed to high SOC content. These results align with those obtained from other Spodosols across the NPCTR (Alexander & Burt, 1996; Alexander et al., 1993; D'Amore et al., 2012; Spinola et al., 2022). For instance, Alexander et al. (1993) reported bulk densities varying from 0.34 to 1.13 g/cm^3 for E and spodic horizons in soils formed from different lithologies in the same region.

The presence of lithologic discontinuities in all study sites, except P2 T–LS, indicates episodes of instability took place before the last cycle of Spodosol development, which is not covered by the Pu isotopes timespan. Despite the steep slopes of our study sites, results from Pu isotopes indicate these soils have remained stable over decadal timescales. This stability contrasts with evidence of gross redistribution indicated by the presence of the colluvial deposits and lithologic discontinuities, which point to more significant soil redistribution events in the past. According to Bormann et al. (1995) and Bowers (1987), forested soils in Southeast Alaska generally have a complex history of soil development mainly due to tree uprooting and to a lesser extent, mass wasting (Bormann et al., 1995; Bowers, 1987). In a broader context of soil redistribution, it is important to differentiate between the mechanisms

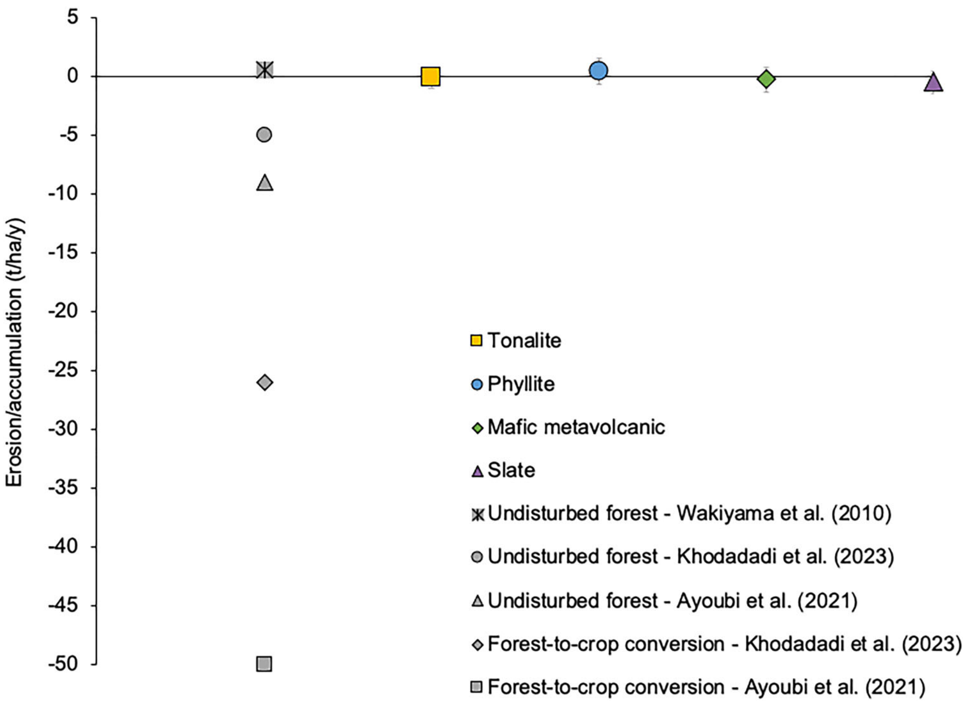

FIGURE 5 Soil redistribution rates (erosion and accumulation) for the study areas with included data from previous research on undisturbed forests and forest-to-crop conversion sites, all located on steep slopes. Negative values indicate soil erosion and positive values indicate soil accumulation. Error bars indicate standard error. Our study rates were calculated using the Profile Distribution Model (Walling & Quine, 1990; Zhang et al., 1990).

and their associated timescales. Mass wasting events, while infrequent, can result in the rapid movement of a large volume of soil, whereas tree throw typically results in localized but recurrent disturbances (Šamonil et al., 2019). In contrast, sheet, rill, and overland erosion are less intense processes that are typically captured by FRNs (IAEA, 2014). Our findings underscore the differential impact of erosive mechanisms over various timescales, offering a window into the complex history of soil dynamics in this region. Future applications of FRNs in natural settings could recognize the layered history of soil movement and use multiple temporal scales and dating techniques when assessing soil stability within forested landscapes, thereby shedding more light into how hillslopes change over time.

4.2 | Source and distribution of Pu isotopes

The ^{240}Pu/^{239}Pu atom ratio is one of the most commonly used tools for tracking the origin of Pu contamination. This isotopic signature can vary considerably depending on its origin (e.g., global fallout, mostly from nuclear tests during the 1960s; regional fallout, usually from power plant accidents, such as Chernobyl in 1986) (Kelley et al., 1999; Ketterer et al., 2004). The ^{240}Pu/^{239}Pu atom average of 0.18 ± 0.005 found in the Juneau soils coincides with the global fallout range of 0.18 ± 0.014 for Northern Hemisphere mid-latitude fallout, indicating a stratospheric/global fallout Pu source without evidence of other potential sources such as Chernobyl or the Nevada Test Site (Kelley et al., 1999; Ketterer et al., 2011; Matisoff et al., 2011). The origin of Pu affects the total $^{239+240}$Pu inventories, which, when aligned with inventories from other reference sites at similar climates, altitudes, and latitudes, serve as an additional approach to evaluate their reliability. Similar Pu signatures have been reported at reference sites in other Northern Hemisphere mid-latitudes soil erosion studies, showing comparable total inventories (Alewell et al., 2014; Musso et al., 2020; Raab et al., 2018; Zollinger et al., 2015). This consistency ensures a uniform baseline of $^{239+240}$Pu inventories in our reference sites. Such uniformity is essential for accurate soil erosion assessments, supporting the assumption that the reference sites have experienced minimal erosion and deposition. Conversely, studies in the Western United States have reported ^{240}Pu/^{239}Pu atom values that indicate regional contamination sources from the Nevada Test Site (Ketterer et al., 2004; Portes et al., 2018). For instance, Portes et al. (2018) reported $^{239+240}$Pu inventories averaging around 200 Bq/m^2 at reference sites, substantially higher than global fallout range found elsewhere (Alewell et al., 2014; Musso et al., 2020; Raab et al., 2018; Zollinger et al., 2015). As expected, the depth distribution of Pu isotopes (Bq/m^2) of the reference sites exhibited a pattern that is typically found at undisturbed sites: higher inventory at the soil surface and a clear exponential decrease with depth (see, e.g., Alewell et al., 2014; Lal et al., 2013; Meusburger et al., 2016; Musso et al., 2020; Portes et al., 2018; Šamonil et al., 2019; Zollinger et al., 2015). The pattern of the exponential depth distribution of Pu isotopes observed in the pedons confirms the suitability of the reference inventories. Over the past few decades, these reference sites have remained undisturbed, unaffected by erosion or deposition, since the initial Pu isotopes fallout input. In the absence of such stable conditions, disturbances in the soil profile could have led to significant perturbations in the Pu depth distribution (FAO/IAEA, 2017). Furthermore, the total $^{239+240}$Pu inventories reported here (i.e., reference inventories of 103 and 126 Bq/m^2) agrees well with the global fallout range of 80–150 Bq/m^2 for reference inventories found in mountain areas in Europe, underscoring the stability of the reference sites (Meusburger et al., 2016, 2020; Musso et al., 2020; Zollinger et al., 2015). Research conducted by Meusburger et al. (2020) illustrates the variability of $^{239+240}$Pu in reference sites across Europe and shows highest inventories in mountainous regions and other areas with high precipitation levels, corresponding with the trends observed at our reference sites. Although we found exponential depth functions for Pu inventories, we observed a greater downward migration of Pu isotopes at our sites (>30-cm deep) compared to other studies (<20-cm deep) (i.e., Ketterer et al., 2004; Musso et al., 2020; Portes et al., 2018; Zollinger et al., 2015). These studies reported negligible Pu inventory below 15- to 20-cm depth. However, we expected higher mobility of Pu in the studied soils due to the fast rates of the eluviation–illuviation processes in Southeast Alaska (Alexander & Burt, 1996; Bormann et al., 1995). Therefore, we sampled down to 30-cm depth to ensure that all $^{239+240}$Pu was included in our samples. Nevertheless, we found 3.4%–5.1% of the total $^{239+240}$Pu inventory was present in the 25–30 cm depth increments, which suggests there may be some Pu inventory below 30 cm and, accordingly, a slight underestimation of the total inventories at all sites.

The vertical mobility of Pu isotopes could be related to the mobility of organic matter, Fe^{3+}, Al^{3+}, and Mn^{3+} oxides downward in the soil profile. Fallout Pu isotopes have a strong affinity for these soil components (Ketterer et al., 2011; Lujaniene et al., 2002; Qiao et al., 2012), which are known to migrate from E horizon to the B horizon by eluviation–illuviation processes. The higher vertical mobility of Pu isotopes in the studied soils could be attributed to rapid rates of podzolization processes in this region. For instance, incipient E horizon and Bs horizons form on well-drained moraines within only 70 years (Alexander & Burt, 1996), which coincides with the timespan since intense global Pu deposition in the 1950s and 1960s. Less pronounced Pu downward migration rates have been reported in Spodosols with slower formation rates. The formation of Spodosols with well-expressed eluvial and illuvial horizons takes place after 3 ka of soil formation in the Swiss Alps (Egli, Fitze et al., 2001; Egli, Mirabella et al., 2001; Zollinger et al., 2015) and after 12 ka of soil formation in the Central Rocky Mountains (Portes et al., 2018).

Despite the higher Pu mobility in Southeast Alaska soils, Pu exhibits a well-developed exponential depth distribution, which is an assumption used by the PDM to convert $^{239+240}$Pu inventories into soil redistribution rates (Alewell et al., 2017; Walling & He, 1999; Walling & Quine, 1990; Zhang et al., 1990). Therefore, the conversion model used here can be considered suitable for estimating soil redistribution rates in Southeast Alaska Spodosols.

4.3 | Soil redistribution rates and slope stability

The calculated $^{239+240}$Pu soil redistribution rates are close to zero (0.43 to −0.51 t/ha/year) indicating that the investigated Spodosols are in a near-stable condition in terms of soil redistribution processes. Soil parent material and related landforms do not appear to affect redistribution processes in these well-developed soils. Our findings agree well with Portes et al. (2018) and Musso et al. (2020) who reported negligible soil redistribution rates for moderately to well-developed soils in mountainous areas. Portes et al. (2018) found that as soils develop from Entisols to Spodosols on granitic moraines, Spodosol development stabilizes hillslopes, and soil redistribution rates become negligible. Musso et al. (2020) reported that even less developed soils (i.e., Inceptisols with a weak to moderate B horizon development) formed from siliceous and calcareous parent materials have reached quasi-stable conditions with erosion rates ranging from 0.3 to 2 t/ha/year.

Our findings also align well with other studies focused on undisturbed forest environments, which reported minimal decadal soil erosion rates in steep hillslopes (Figure 5). Wakiyama et al. (2010) calculated ^{137}Cs soil redistribution rates ranging from 0.58 to 1.24 t/ha/year in steep hillslopes (40%) in coniferous forests in Japan. Kaste et al. (2007) reported steady-state denudation rates and consequently low erosion rates for Spodosols located on steep slopes in a mixed temperate forest in New England. Conversely, other studies have reported higher soil erosion rates for steep hillslopes in undisturbed forest environments, suggesting a non-steady state condition. For example, Khodadadi et al. (2023) and Ayoubi et al. (2021) estimated soil erosion rates using ^{137}Cs for forested hillslopes in oak forests in western Iran and found rates of 5 and 9 t/ha/year, respectively (Figure 5). These studies showed that following the conversion from the oak forest into agricultural ecosystems, erosion rates increased by five times, up to roughly 26 t/ha/year in Khodadadi et al.

(2023) and 50 t/ha/year in Ayoubi et al. (2021), indicating a substantial impact of deforestation on slope stability.

The stability of these slopes in Southeast Alaska has significant implications for the storage and persistence of SOC. Hunter et al. (2024) demonstrate that both total SOC stocks and the mineral-associated fraction of SOC decrease exponentially with increasing erosion rates in hilly and mountainous areas in the Northwest Pacific coast. Thick and highly altered soils, such as the Spodosols across Southeast Alaska, exhibit low erosion rates and provide long mean residence times allowing higher mineral association of SOC (Hunter et al., 2023, 2024), therefore, acting as carbon sinks. Considering the characteristics of the Southeast Alaska environment, the stabilization of the steep slopes in Southeast Alaska could be related to the interplay between soil development, root systems, and vegetation cover. The pedons we studied have a high content of coarse fragments and exhibit loamy textures, blocky structures, and high root densities. These characteristics increase soil porosity, promote water infiltration, and therefore inhibit erosion processes. Furthermore, superficial roots prevent soil erosion by excretioning exudates, which induce soil aggregation (Amézketa, 1999; Gyssels et al., 2005; Hudek et al., 2017) and mechanical fixation of soil particles (Greenway, 1987; Heilman & Gass, 1974). Moreover, roots increase shear strength in soils located on steep slopes by anchoring the soil mass (Swanston, 1974). Vegetation also plays an important role in protecting the soil surface from water erosion. The dense conifer forest, understory, and moss cover intercept raindrops, therefore enhancing water infiltration and preventing soil detachment and redistribution processes (Gyssels et al., 2005; Musso et al., 2020; Portes et al., 2018). Therefore, these combined factors seem to contribute to the resistance of soils against erosion and deposition processes on steep slopes across varied lithologies in the region.

5 | CONCLUSIONS

Our study presents the first quantification of soil redistribution rates in temperate rainforests of Southeast Alaska to understand how lithology and landform control soil development and soil erosion processes. Overall, all soils share similar morphological and chemical properties regardless of soil parent material (i.e., tonalite, phyllite, mafic metavolcanic, and slate). The $^{239+240}$Pu results support our hypothesis that deep Spodosols formed from different lithologies and landforms across the Juneau area are in a steady-state condition in terms of medium-term soil redistribution rates. Spodosols showed negligible $^{239+240}$Pu soil redistribution rates, ranging from erosion rates of 0.51 t/ha/year to deposition rates of 0.43 t/ha/year, which suggests that these surfaces are stable on a decadal timescale. The interplay between soil development, root systems, and vegetation cover contributes to the stabilization of the steep slopes. Therefore, our results suggest that lithology and landform do not seem to affect soil redistribution rates in Spodosols located on convex steep slopes in Southeast Alaska.

AUTHOR CONTRIBUTIONS

Raquel Portes: Conceptualization; data curation; formal analysis; funding acquisition; investigation; methodology; project administration; writing—original draft. **Diogo Spinola**: Conceptualization; formal analysis; investigation; methodology; writing—original draft; writing—review and editing. **Michael E. Ketterer**: Data curation; methodology; resources; writing—review and editing. **Markus Egli**: Methodology; writing—review and editing. **Rebecca A. Lybrand**: Methodology; writing—review and editing. **Jennifer Fedenko**: Methodology; writing—review and editing. **Frances Biles**: Software; writing—review and editing. **Thomas P. Trainor**: Investigation; resources; writing—review and editing. **Ashlee Dere**: Investigation; writing—review and editing. **David V. D'Amore**: Conceptualization; funding acquisition; investigation; resources; supervision; writing—original draft; writing—review and editing.

ACKNOWLEDGMENTS

We acknowledge that the study sites in Juneau, AK, are located on the unceded land of the Tlingit people. We thank Randy Hesser, John Wright, and Justin Crotteau for their assistance during the fieldwork and Tim Howe (Alaska Stable Isotope Facility-University of Alaska Fairbanks) for the soil organic carbon measurements. We are also thankful to Pauline Plumb, Mark Luke, and Emily Whitney for their logistical support at the Juneau Forestry Science Lab, and to the Dry Runs and Peer Review Subcommittee of the GeoLatinas and Lynsey MacLeary (Isotope Editing) for comments and proofreading an earlier version of the manuscript. We also thank two anonymous reviewers for their valuable feedback.

CONFLICT OF INTEREST STATEMENT

The authors declare no conflicts of interest.

ORCID

Raquel Portes https://orcid.org/0000-0003-2673-4232
Diogo Spinola https://orcid.org/0000-0003-3525-9461
Rebecca A. Lybrand https://orcid.org/0000-0001-7811-9093

REFERENCES

Alewell, C., Meusburger, K., Juretzko, G., Mabit, L., & Ketterer, M. E. (2014). Suitability of $^{239+240}$Pu and ^{137}Cs as tracers for soil erosion assessment in mountain grasslands. *Chemosphere*, *103*, 274–280. https://doi.org/10.1016/j.chemosphere.2013.12.016

Alewell, C., Pitois, A., Meusburger, K., Ketterer, M., & Mabit, L. (2017). $^{239+240}$Pu from "contaminant" to soil erosion tracer: Where do we stand? *Earth-Science Reviews*, *172*(117), 107–123. https://doi.org/10.1016/j.earscirev.2017.07.009

Alexander, E. B., & Burt, R. (1996). Soil development on moraines of Mendenhall Glacier, southeast Alaska. 1. The moraines and soil morphology. *Geoderma*, *72*(1–2), 1–17. https://doi.org/10.1016/0016-7061(96)00021-3

Alexander, E. B., Shoji, S., & West, R. (1993). Andic soil properties of Spodosols in nonvolcanic materials of southeast Alaska. *Soil Science Society of America Journal*, *475*, 472–475. https://doi.org/10.2136/sssaj1993.03615995005700020029x

Amézketa, E. (1999). Soil aggregate stability: A review. *Journal of Sustainable Agriculture*, *14*(3), 83–151. https://doi.org/10.1300/J064v14n02

Ayoubi, S., Sadeghi, N., Abbaszadeh Afshar, F., Abdi, M. R., Zeraatpisheh, M., & Rodrigo-Comino, J. (2021). Impacts of oak deforestation and rainfed cultivation on soil redistribution processes across hillslopes using ^{137}Cs techniques. *Forest Ecosystems*, *8*(1), Article 32. https://doi.org/10.1186/s40663-021-00311-1

Bormann, B. T., Spaltenstein, H., Mcclellan, M. H., Ugolini, F. C., Cromack, K., Jr., & Nay, S. M. (1995). Rapid soil development after windthrow disturbance in pristine forests. *Journal of Ecology*, *83*(5), 747–757. https://doi.org/10.2307/2261411

Bouhlassa, S., & Bouhsane, N. (2023). Assessment of the impacts of land-use change and slope position on soil loss by magnetic susceptibility-based models. *International Journal of Sediment Research*, *38*(3), 455–468. https://doi.org/10.1016/j.ijsrc.2022.11.006

Bowers, F. H. (1987). *Effects of windthrow on soil properties and spatial variability in southeast Alaska* [Doctoral dissertation, University of Washington].

Calitri, F., Sommer, M., Norton, K., Temme, A., Brandová, D., Portes, R., Christl, M., Ketterer, M. E., & Egli, M. (2019). Tracing the temporal evolution of soil redistribution rates in an agricultural landscape using $^{239+240}$Pu and ^{10}Be. *Earth Surface Processes and Landforms*, *44*(9), 1783–1798. https://doi.org/10.1002/esp.4612

Carpenter, D. N., Bockheim, J. G., & Reich, P. F. (2014). Soils of temperate rainforests of the North American Pacific Coast. *Geoderma*, *230–231*, 250–264. https://doi.org/10.1016/j.geoderma.2014.04.023

Carrara, P. E., Ager, T. A., & Baichtal, J. F. (2007). Possible refugia in the Alexander Archipelago of southeastern Alaska during the late Wisconsin glaciation. *Canadian Journal of Earth Sciences*, *44*, 229–244. https://doi.org/10.1139/e06-081

Chandler, R. F. (1942). The time required for podzol profile formation as evidenced by the Mendenhali glacial deposits near Juneau, Alaska. *Soil Science Society of America Journal*, *7*, 454–459. https://doi.org/10.2136/sssaj1943.036159950007000C0077x

Chen, S., Zhang, G., Zhu, P., Wang, C., & Wan, Y. (2022). Impact of slope position on soil erodibility indicators in rolling hill regions of northeast China. *Catena*, *217*, 106475. https://doi.org/10.1016/j.catena.2022.106475

Cremeens, D. L., & Mokma, D. L. (1986). Argillic horizon expression and classification in the soils of two Michigan hydrosequences. *Soil Science Society of America Journal*, *50*, 1002–1007. https://doi.org/10.2136/sssaj1986.03615995005000040034x

Crocker, R. L., & Dickson, B. A. (1957). Soil development on the recessional moraines of the Herbert and Mendenhall glaciers, south-eastern Alaska. *Journal of Ecology*, *45*(1), 169–185. https://doi.org/10.2307/2257083

D'Amore, D. V., Fellman, J. B., Edwards, R. T., Hood, E., & Ping, C.-L. (2012). Hydropedology of the North American coastal temperate rainforest. In H. Lin (Ed.), *Hydropedology: Synergistic integration of soil science and hydrology* (pp. 351–380). Academic Press.

D'amore, D. V., Ping, C.-L., & Herendeen, P. A. (2015). Hydromorphic soil development in the coastal temperate rainforest of Alaska. *Soil Science Society of America Journal*, *79*(2), 698–709. https://doi.org/10.2136/sssaj2014.08.0322

De Coninck, F. (1980). Major mechanisms in formation of spodic horizons. *Geoderma*, *24*, 101–128. https://doi.org/10.1016/0016-7061(80)90038-5

Egli, M., Fitze, P., & Mirabella, A. (2001). Weathering and evolution of soils formed on granitic, glacial deposits: Results from chronosequences of Swiss alpine environments. *Catena*, *45*(1), 19–47. https://doi.org/10.1016/S0341-8162(01)00138-2

Egli, M., Mirabella, A., & Fitze, P. (2001). Clay mineral formation in soils of two different chronosequences in the Swiss Alps. *Geoderma*, *104*(1–2), 145–175. https://doi.org/10.1016/S0016-7061(01)00079-9

FAO/IAEA. (2017). Use of ^{137}Cs for soil erosion assessment. In E. Fulajtar, L. Mabit, C. S. Renschler, & A. Lee Z. Yi (Eds.), *Joint FAO/IAEA programme: Nuclear techniques in food and agriculture*. Food and Agriculture Organization of the United Nations, International Atomic Energy Agency.

Gee, G. W., & Bauder, J. W. (1986). Particle-size analysis. In A. Klute (Ed.), *Methods of soil analysis: Part 1—Physical and mineralogical methods* (pp. 383–411). SSSA. https://doi.org/10.2136/sssabookser5.1.2ed.c15

Gehrels, G. E., & Berg, H. C. (1992). *Geologic map of southeastern Alaska: U.S. Geological Survey miscellaneous investigations series map 1867, 1 sheet, scale 1:600,000*. State of Alaska Department of Natural Resources. https://dggs.alaska.gov/pubs/id/12916

Greenway, D. R. (1987). Vegetation and slope stability. In M. Anderson, & K. Richards (Eds.), *Slope stability: Geotechnical engineering and geomorphology* (pp. 187–230). Wiley.

Gyssels, G., Poesen, J., Bochet, E., & Li, Y. (2005). Impact of plant roots on the resistance of soils to erosion by water: A review. *Progress in Physical Geography: Earth and Environment*, *29*(2), 189–217. https://doi.org/10.1191/0309133305pp443ra

Heilman, P. E., & Gass, C. R. (1974). Parent materials and chemical properties of mineral soils in southeast Alaska. *Soil Science*, *117*(1), 21–27. https://doi.org/10.1097/00010694-197401000-00003

Hudek, C., Stanchi, S., D'amico, M., & Freppaz, M. (2017). Quantifying the contribution of the root system of alpine vegetation in the soil aggregate stability of moraine. *International Soil and Water Conservation Research*, *5*(1), 36–42. https://doi.org/10.1016/j.iswcr.2017.02.001

Huggett, R. J. (1975). Soil landscape systems: A model of soil genesis. *Geoderma*, *13*, 1–22. https://doi.org/10.1016/0016-7061(75)90035-X

Hunter, B. D., Roering, J. J., Almond, P. C., Chadwick, O. A., Polizzotto, M. L., & Silva, L. C. R. (2023). Pedogenic pathways and deep weathering controls on soil organic carbon in Pacific Northwest forest soils. *Geoderma*, *436*, 116531. https://doi.org/10.1016/j.geoderma.2023.116531

Hunter, B. D., Roering, J. J., Silva, L. C. R., & Moreland, K. C. (2024). Geomorphic controls on the abundance and persistence of soil organic carbon pools in erosional landscapes. *Nature Geoscience*, *17*(2), 151–157. https://doi.org/10.1038/s41561-023-01365-2

IAEA. (2014). Assessment of soil erosion and sedimentation: The role of fallout radionuclides. In L. Mabit, F. Zapata, M. Benmansour, C. Bernard, G. Dercon, D. E. Walling (Eds.), *Guidelines for using fallout radionuclides to assess erosion and effectiveness of soil conservation strategies* (IAEA-TECDOC-1741) (pp. 3–26). IAEA.

Kaste, J. M., Heimsath, A. M., & Bostick, B. C. (2007). Short-term soil mixing quantified with fallout radionuclides. *Geology*, *35*(3), 243–246. https://doi.org/10.1130/G23355A.1

Kelley, J. M., Bond, L. A., & Beasley, T. M. (1999). Global distribution of Pu isotopes and ^{237}Np. *Science of the Total Environment*, *237/238*, 483–500. https://doi.org/10.1016/S0048-9697(99)00160-6

Ketterer, M. E., Hafer, K. M., & Mietelski, J. W. (2004). Resolving Chernobyl vs. global fallout contributions in soils from Poland using plutonium atom ratios measured by inductively coupled plasma mass spectrometry. *Journal of Environmental Radioactivity*, *73*(2), 183–201. https://doi.org/10.1016/j.jenvrad.2003.09.001

Ketterer, M. E., Zheng, J., & Yamada, M. (2011). Applications of transuranics as tracers and chronometers in the environment. In M. Baskaran (Ed.), *Handbook of environmental isotope geochemistry* (pp. 395–418). Springer.

Khodadadi, M., Alewell, C., Mirzaei, M., Ehssan-Malahat, E., Asadzadeh, F., Strauss, P., & Meusburger, K. (2023). Understanding deforestation impacts on soil erosion rates using ^{137}Cs, $^{239+240}$Pu, and ^{210}Pb$_{ex}$ and soil physicochemical properties in western Iran. *Journal of Environmental Radioactivity*, *257*, 107078. https://doi.org/10.1016/j.jenvrad.2022.107078

King, G. J., Acton, D. F., & St Arnaud, R. J. (1983). Soil-landscape analysis in relation to soil distribution and mapping at a site within the Weyburn association. *Canadian Journal of Soil Science*, *63*, 657–670. https://doi.org/10.4141/cjss83-067

Lal, R., & Elliot, W. (1994). Erodibility and erosivity. In R. Lal (Ed.), *Soil erosion research method* (pp. 181–208). Soil and Water Conservation Society, St. Lucie Press.

Lal, R., Tims, S. G., Fifield, L. K., Wasson, R. J., & Howe, D. (2013). Applicability of ^{239}Pu as a tracer for soil erosion in the wet-dry tropics of northern Australia. *Nuclear Instruments and Methods in Physics Research Section B: Beam Interactions with Materials and Atoms*, *294*, 577–583. https://doi.org/10.1016/j.nimb.2012.07.041

Lesnek, A. J., Briner, J. P., Baichtal, J. F., & Lyles, A. S. (2020). New constraints on the last deglaciation of the Cordilleran Ice Sheet in coastal southeast Alaska. *Quaternary Research*, *96*, 140–160. https://doi.org/10.1017/qua.2020.32

Lesnek, A. J., Briner, J. P., Lindqvist, C., Baichtal, J. F., & Heaton, T. H. (2018). Deglaciation of the pacific coastal corridor directly preceded the human colonization of the Americas. *Science Advances*, *4*(5), eaar5040. https://doi.org/10.1126/sciadv.aar5040

Li, M., Shi, X., Shen, Z., Yang, E., Bao, H., & Ni, Y. (2019). Effect of hillslope aspect on landform characteristics and erosion rates. *Environmental Monitoring and Assessment*, *191*(9), Article 598. https://doi.org/10.1007/s10661-019-7760-1

Liu, B. Y., Nearing, M. A., Shi, P. J., & Jia, Z. W. (2000). Slope length effects on soil loss for steep slopes. *Soil Science Society of America Journal*, *64*(5), 1759–1763. https://doi.org/10.2136/sssaj2000.6451759x

Lujaniene, G., Plukis, A., Kimtys, E., Remeikis, V., Jankünaite, D., & Ogorodnikov, B. I. (2002). Study of ^{137}Cs, ^{90}Sr, ^{239,240}Pu, ^{238}Pu and ^{241}Am behavior in the Chernobyl soil. *Journal of Radioanalytical and Nuclear Chemistry*, *251*, 59–68. https://doi.org/10.1023/A:1015185011201

Martz, L. W. (1992). The variation of soil erodibility with slope position in a cultivated Canadian prairie landscape. *Earth Surface Processes and Landforms*, *17*(6), 543–556. https://doi.org/10.1002/esp.3290170602

Matisoff, G., Ketterer, M. E., Rosén, K., Mietelski, J. W., Vitko, L. F., Persson, H., & Lokas, E. (2011). Downward migration of Chernobyl-derived radionuclides in soils in Poland and Sweden. *Applied Geochemistry*, *26*(1), 105–115. https://doi.org/10.1016/j.apgeochem.2010.11.007

Mcnicol, G., Bulmer, C., D'amore, D., Sanborn, P., Saunders, S., Giesbrecht, I., Arriola, S. G., Bidlack, A., Butman, D., & Buma, B. (2019). Large, climate-sensitive soil carbon stocks mapped with pedology-informed machine learning in the North Pacific coastal temperate rainforest. *Environmental Research Letters*, *14*(1), 014004. https://doi.org/10.1088/1748-9326/aaed52

Meusburger, K., Evrard, O., Alewell, C., Borrelli, P., Cinelli, G., Ketterer, M., Mabit, L., Panagos, P., Van Oost, K., & Ballabio, C. (2020). Plutonium aided reconstruction of caesium atmospheric fallout in European topsoils. *Scientific Reports*, *10*(1), Article 11858. https://doi.org/10.1038/s41598-020-68736-2

Meusburger, K., Mabit, L., Ketterer, M., Park, J.-H., Sandor, T., Porto, P., & Alewell, C. (2016). A multi-radionuclide approach to evaluate the suitability of $^{239+240}$Pu as soil erosion tracer. *Science of the Total Environment*, *566–567*, 1489–1499. https://doi.org/10.1016/j.scitotenv.2016.06.035

Meusburger, K., Porto, P., Mabit, L., La Spada, C., Arata, L., & Alewell, C. (2018). Excess Lead-210 and Plutonium-239+240: Two suitable radiogenic soil erosion tracers for mountain grassland sites. *Environmental Research*, *160*, 195–202. https://doi.org/10.1016/j.envres.2017.09.020

Mikutta, R., Kleber, M., Kaiser, K., & Jahn, R. (2005). Review: Organic matter removal from soils using hydrogen peroxide, sodium hypochlorite, and sodium peroxodisulfate. *Soil Science Society of America Journal*, *69*(1), 120–135. https://doi.org/10.2136/sssaj2005.0120

Miller, R. D. (1975). *Surficial geologic map of the Juneau urban area and vicinity, Alaska: U.S. Geological Survey miscellaneous investigations series map 885, 1 sheet, scale 1:48,000*. State of Alaska Department of Natural Resources. https://dggs.alaska.gov/pubs/id/12956

Musielok, Ł., Drewnik, M., Szymański, W., Stolarczyk, M., Gus-Stolarczyk, M., & Skiba, M. (2021). Conditions favoring local podzolization in soils developed from flysch regolith—A case study from the Bieszczady Mountains in southeastern Poland. *Geoderma*, *381*, 114667. https://doi.org/10.1016/j.geoderma.2020.114667

Musso, A., Ketterer, M. E., Greinwald, K., Geitner, C., & Egli, M. (2020). Rapid decrease of soil erosion rates with soil formation and vegetation development in periglacial areas. *Earth Surface Processes and Landforms*, *45*(12), 2824–2839. https://doi.org/10.1002/esp.4932

NOOA. (2020). *1991-2020 Climate normals*. https://www.weather.gov/tbw/newnormals

Owens, P. N. (2020). Soil erosion and sediment dynamics in the Anthropocene: A review of human impacts during a period of rapid global environmental change. *Journal of Soils and Sediments*, *20*(12), 4115–4143. https://doi.org/10.1007/s11368-020-02815-9

Portes, R., Dahms, D., Brandová, D., Raab, G., Christl, M., Kühn, P., Ketterer, M., & Egli, M. (2018). Evolution of soil erosion rates in alpine soils of the Central Rocky Mountains using fallout Pu and δ^{13}C. *Earth & Planetary Science Letters*, *496*, 257–269. https://doi.org/10.1016/j.epsl.2018.06.002

Portes, R. D. C., Spinola, D. N., Reis, J. S., Ker, J. C., Costa, L. M. D., Fernandes Filho, E. I., Kühn, P., & Schaefer, C. E. G. R. (2016). Pedogenesis across a climatic gradient in tropical high mountains, Cordillera Blanca—Peruvian Andes. *Catena*, *147*, 441–452. https://doi.org/10.1016/j.catena.2016.07.027

Pudasaini, S. P., & Krautblatter, M. (2021). The mechanics of landslide mobility with erosion. *Nature Communications*, *12*(1), Article 6793. https://doi.org/10.1038/s41467-021-26959-5

Qiao, J., Hansen, V., Hou, X., Aldahan, A., & Possnert, G. (2012). Speciation analysis of ^{129}I, ^{137}Cs, ^{232}Th, ^{238}U, ^{239}Pu and ^{240}Pu in environmental soil and sediment. *Applied Radiation and Isotopes*, *70*, 1698–1708. https://doi.org/10.1016/j.apradiso.2012.04.006

Quine, T. A., & Walling, D. E. (1991). Rates of soil erosion on arable fields in Britain: Quantitative data from caesium-137 measurements. *Soil Use and Management*, *7*, 169–176. https://doi.org/10.1111/j.1475-2743.1991.tb00870.x

Raab, G., Scarciglia, F., Norton, K., Dahms, D., Brandová, D., De Castro Portes, R., Christl, M., Ketterer, M. E., Ruppli, A., & Egli, M. (2018). Denudation variability of the Sila Massif upland (Italy) from decades to millennia using ^{10}Be and $^{239+240}$Pu. *Land Degradation & Development*, *29*, 3736–3752. https://doi.org/10.1002/ldr.3120

Šamonil, P., Egli, M., Steinert, T., Norton, K., Abiven, S., Daněk, P., Hort, L., Brandová, D., Christl, M., & Tikhomirov, D. (2019). Soil denudation rates in an old-growth mountain temperate forest driven by tree uprooting dynamics, Central Europe. *Land Degradation & Development*, *31*(2), 222–239. https://doi.org/10.1002/ldr.3443

Schaetzl, R. J. (1991). A lithosequence of soils in extremely gravelly, dolomitic parent materials, Bois Blanc Island, Lake Huron. *Geoderma*, *48*(3–4), 305–320. https://doi.org/10.1016/0016-7061(91)90050-4

Schaetzl, R. J. (1998). Lithologic discontinuities in some soils on drumlins: Theory, detection, and application. *Soil Science*, *163*(7), 570–590. https://doi.org/10.1097/00010694-199807000-00006

Schaetzl, R. J., & Anderson, S. (2005). *Soils: Genesis and geomorphology*. Cambridge University Press.

Schimmack, W., Auerswald, K., & Bunzl, K. (2001). Can $^{239+240}$Pu replace ^{137}Cs as an erosion tracer in agricultural landscapes contaminated with Chernobyl fallout? *Journal of Environmental Radioactivity*, *53*(1), 41–57. https://doi.org/10.1016/S0265-931X(00)00117-X

Schoeneberger, P. J., Wysocki, D. A., Benham, E. C., & Soil Staff, S. (2012). *Field book for describing and sampling soils* (3rd ed.). Natural Resources Conservation Service, National Soil Survey Center.

Schwertmann, U. (1964). The differentiation of iron oxides in soil by extraction with ammonium oxalate solution. *Zeitschrift für Pflanzenernährung, Düngung, Bodenkunde*, *105*, 194–202. https://doi.org/10.1002/jpln.3591050303

Singleton, G. A., & Lavkulich, L. M. (1987). Phosphorus transformations in a soil chronosequence, Vancouver Island, British Columbia. *Canadian Journal of Soil Science*, *67*, 787–793.

Soil Survey Staff. (2014a). *Keys to soil taxonomy* (12th ed.). USDA-NRCS.

Soil Survey Staff. (2014b). Soil survey field and laboratory methods manual. In R. Burt, & S. S. Staff (Eds.), *Soil survey investigations report no. 51, version 2.0*. USDA-NRCS.

Spinola, D., Portes, R., Fedenko, J., Lybrand, R., Dere, A., Biles, F., Trainor, T., Bowden, M. E., & D'amore, D. (2022). Lithological controls on soil geochemistry and clay mineralogy across Spodosols in the coastal temperate rainforest of southeast Alaska. *Geoderma*, *428*, 116211. https://doi.org/10.1016/j.geoderma.2022.116211

Swanston, D. N. (1974). Soil mass movement. In *The forest ecosystem of southeast Alaska* (Pacific Northwest Research Station General Technical Report PNW-GTR-17). USDA Forest Service.

Ugolini, F. C., & Dahlgren, R. (1987). The mechanism of podzolization as revealed by soil solution studies. In D. Righi, & A. Chauvel (Eds.), *Podzols et podzolisation* (pp. 195–203). Association Française pour l'Etude du Sol and Institut National de la Recherche Agronomique.

USDA. (1996). *Landforms of the Alaska region classification guide*. USDA Forest Service.

Velasco, H., Astorga, R. T., Joseph, D., Antoine, J. S., Mabit, L., Toloza, A., Dercon, G., & Walling, D. E. (2018). Adapting the caesium-137 technique to document soil redistribution rates associated with traditional cultivation practices in Haiti. *Journal of Environmental Radioactivity*, *183*, 7–16. https://doi.org/10.1016/j.jenvrad.2017.12.008

Wakiyama, Y., Onda, Y., Mizugaki, S., Asai, H., & Hiramatsu, S. (2010). Soil erosion rates on forested mountain hillslopes estimated using ^{137}Cs and $^{210}Pb_{ex}$. *Geoderma*, *159*(1–2), 39–52. https://doi.org/10.1016/j.geoderma.2010.06.012

Walling, D. E., & He, Q. (1999). Improved models for estimating soil erosion rates from cesium-137 measurements. *Journal of Environmental Quality*, *28*, 611–622. https://doi.org/10.2134/jeq1999.00472425002800020027x

Walling, D. E., & Quine, T. A. (1990). Calibration of caesium-137 measurements to provide quantitative erosion rate data. *Land Degradation & Development*, *2*, 161–175. https://doi.org/10.1002/ldr.3400020302

Wilken, F., Fiener, P., Ketterer, M., Meusburger, K., Muhindo, D. I., van Oost, K., & Doetterl, S. (2021). Assessing soil erosion of forest and cropland sites in wet tropical Africa using $^{239+240}$Pu fallout radionuclides. *SOIL*, *95*, 399–414.

Wilken, F., Ketterer, M., Koszinski, S., Sommer, M., & Fiener, P. (2020). Understanding the role of water and tillage erosion from $^{239+240}$Pu tracer measurements using inverse modelling. *SOIL*, *6*, 549–564.

Xu, Y., Qiao, J., Hou, X., & Pan, S. (2013). Plutonium in soils from northeast China and its potential application for evaluation of soil erosion. *Scientific Reports*, *3*, Article 3506. https://doi.org/10.1038/srep03506

Zhang, X., Higgitt, D. L., & Walling, D. E. (1990). A preliminary assessment of the potential for using caesium-137 to estimate rates of soil erosion in the Loess Plateau of China. *Hydrological Sciences Journal*, *35*, 43–252.

Zollinger, B., Alewell, C., Kneisel, C., Meusburger, K., Brandová, D., Kubik, P., Schaller, M., Ketterer, M., & Egli, M. (2015). The effect of permafrost on time-split soil erosion using radionuclides (^{137}Cs, $^{239+240}$Pu, meteoric ^{10}Be) and stable isotopes (δ^{13}C) in the eastern Swiss Alps. *Journal of Soils and Sediments*, *15*(6), 1400–1419. https://doi.org/10.1007/s11368-014-0881-9

How to cite this article: Portes, R., Spinola, D., Ketterer, M. E., Egli, M., Lybrand, R. A., Fedenko, J., Biles, F., Trainor, T. P., Dere, A., & D'Amore, D. V. (2024). Assessing decadal soil redistribution rates using 239+240Pu across diverse lithologies in Southeast Alaska. *Soil Science Society of America Journal*, *88*, 1659–1677. https://doi.org/10.1002/saj2.20732